UNSTEADY RANSE AND DETACHED-EDDY SIMULATIONS OF CAVITATING FLOW

Matthias Maasch, Osman Turan, Mahdi Khorasanchi

Department of Naval Architecture and Marine Engineering, University of Strathclyde, 100 Montrose Street, Glasgow G4 0LZ, UK, matthias.maasch@strath.ac.uk, o.turan@strath.ac.uk, mahdi.khorasanchi@strath.ac.uk

ABSTRACT

The Twisted Delft Hydrofoil and the Potsdam Propeller Test Case (PPTC) were used to analyse and compare the capabilities of Reynolds-Averaged Navier Stokes Equations simulations (RANSE simulations) and detached-eddy simulations (DES) to predict three-dimensional cavitating flow. Although the RANSE simulations were able to predict the lift and drag forces in reasonable agreement with the experiments, it has been shown that the accurate numerical simulation of cavitational flow requires the use of an advanced model such as the SST k-omega detached-eddy model.

Keywords: URANSE, DES, Cavitation, Delft Hydrofoil, PPTC

1. INTRODUCTION

For the marine industry as well as the marine R&D Computational Fluid Dynamics (CFD), combined with Experimental Fluid Dynamics (EFD), are key methods to predict the performance of flow-exposed geometry to analyse where efficiency gets lost. On that basis it is possible to improve the geometry design in terms of energy efficiency and safety. Whereas model tests are well established and widely used in the marine industry for more than 100 years, CFD, as a much younger field of science, is still a challenge and needs ongoing research. Most of today's CFD codes are able to predict flow physics fairly well. Nevertheless, there are limitations when it is required to predict turbulent flow in very small scales of space and time. Cavitation, the formation and destruction of vapour cavities in water, is a flow phenomenon which highly depends on those small scales. Predicting the details of cavitational flow becomes crucial for performing e.g. comprehensive hydrodynamic form optimisation in marine industrial applications, especially for appendages geometry such as propeller and rudder.

Whereas widely used approaches such as Lifting Line and Lifting Surface codes are fairly able to predict the cavitation development on surfaces, these codes have their weakness in predicting shedding cavitation phenomena and the collapse of cavitation bubbles in the wake field of the ship, both crucial for investigating the influence of cavitation on the hull and appendages (Boorsma and Whitworth, 2011). The main effects of cavitation are vibration, material erosion and also efficiency losses due to propeller thrust breakdown. In order to simulate these effects it is necessary to accurately predict the flow on the propeller surface near the propeller tips. For that purpose the following numerical methods are suitable:

1. Reynolds-Averaged Navier Stokes Equations Simulation – RANSE simulation
2. Large Eddy Simulation – LES
3. Detached Eddy Simulation – DES
4. Direct Numerical Simulation – DNS

While RANSE simulations use equations which give a good estimations of the turbulent flow physics, LES and DNS resolve the governing equations and thus give more insight into the flow details. The DES combines the RANSE method, which gives solutions in a reasonable period of time by modelling

the attached turbulent flow near to the geometry wall, with the LES method, which actually solves the free flow physics. Salvatore (Salvatore et al., 2009) showed, that LES, using very small steps in time and space, resolve more flow structures than the RANSE simulations. This is desirable, but in addition Muscari (Muscari et al., 2012) mentioned that LES and DNS require an unpractical high grid resolution in the boundary layer region of the geometry.

To make use of the advantages of LES and DNS the numerical grid must be fine as well as the solver's time step has to be kept very small, both resulting in a high number of time steps necessary to predict the small scale flow structures. These requirements have a major impact on the necessary computational time. Muscari (Muscari et al., 2012) pointed out, although the DNS approach is available, the use of this method is due to very high computational times out of reach, at least for time-critical industrial applications. Ashton (Ashton et al., 2014) proposed that LES will become a feasible industrial application in 2045. For DNS even the year 2080 is assumed. These rough estimations obviously are based on the future development of computational power and improvements in software development, e.g. parallel computing. Considering these assumptions, the DES seems to be a good alternative to keep the computational time in a reasonable frame but also to solve the flow structures as detailed as necessary. Muscari (Muscari et al., 2012) showed that in fact DES solve physics on a smaller scale and thus makes the results more reliable compared to RANSE simulations.

As the effects of excessive cavitating flow are predominately negative for the ship's efficiency and the accuracy of numerical cavitation prediction isn't always in line with experimental results gained in model tests, there is still the need to validate and to improve the application of the above mentioned numerical simulation methods. A method often used is to validate different test case results. Such test cases were carried out under well-defined conditions for different types of flow-exposed geometry. The results of these tests are publicly available.

2. METHODOLOGY

Two well-known test cases, namely the Twisted Delft Hydro Foil and the Potsdam Propeller Test Case (PPTC), were used to analyse and compare the capabilities of RANSE simulations and detached-eddy simulations to predict cavitation. Therefore the RANS simulations were run first to get a general idea of how to setup the mesh and the physics. After satisfying results were gained the detached-eddy simulations were run. Finally the different approaches were compared in terms of the accuracy of the predicted flow features.

As detached-eddy simulations require a denser grid than RANSE simulations, a mesh test procedure was applied to the RANSE simulations. The test evaluated the numerical mesh for its ability to resolve the smallest scales of turbulence. Therefore the turbulence length scale $\mathrm{l_{k\omega}}$ (1) for the k-omega SST turbulence model, considering a model factor C_μ, the turbulent kinetic energy k and the specific dissipation rate ω, is calculated in relation to the local length of the cuboid cells l_C (2), derived from the respective cell volume $\mathrm{V_C}$.

$$\mathrm{l_{k\omega}} = {C_\mu}^{-1/4}\frac{\sqrt{\mathrm{k}}}{\omega} \tag{1}$$

$$\mathrm{l_C} = \sqrt[3]{\mathrm{V_C}} \tag{2}$$

The resulting function describes the turbulence length ratio $\mathrm{r_l}$on the numerical mesh (3). Values of $\mathrm{r_l} < 1$ would indicate that the mesh needs further refinement. The factor a scales the turbulence length ratio (see Figure 1). A value of $a = 1$ would resolve the small eddies using one cell, a value of

$a = 4$ would use four cells which is considered to be more accurate. A value smaller than one (e.g. $a = 0.25$) is not sufficient to resolve the smallest scales as one eddy would be four times smaller than the cell. It is recommended to solve the small scale eddies with at least two cells being reflected in a value of $a = 2$ (recommended value provided by cd-adapco support).

$$r_l = \frac{l_{k\omega}}{a \cdot l_C} \tag{3}$$

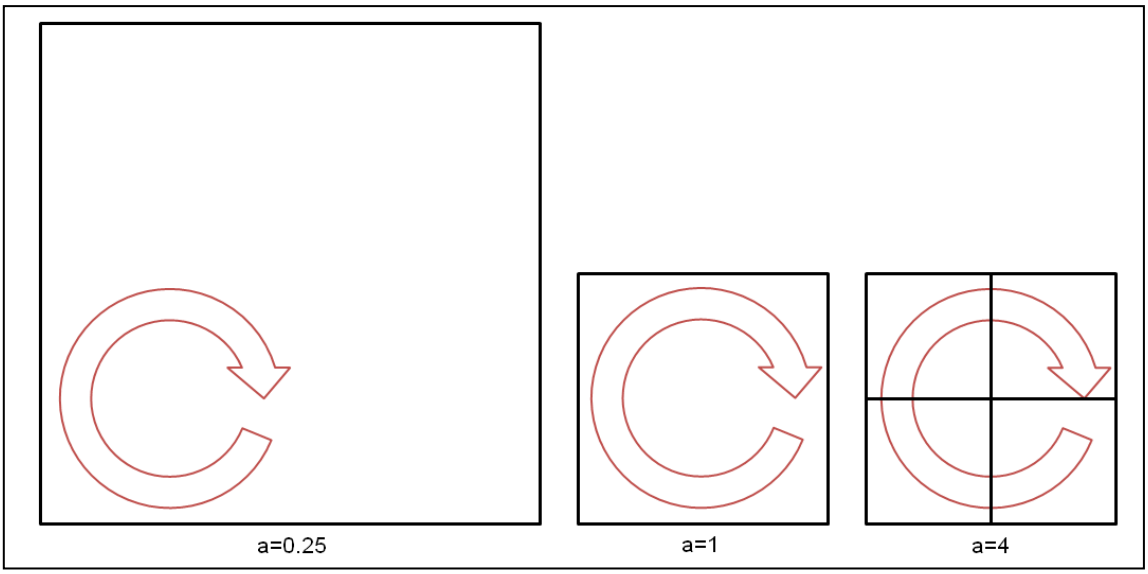

Figure 1 – The influence of the factor a on the turbulence length ratio

All simulations were run until the computed forces and moments oscillated around a constant value and the normalized residuals indicated a converged solution. As recommended by the ITTC the respective time step of the implicit unsteady solver was chosen so that the main flow features were resolved in an acceptable range (ITTC, 2011). For the simulations of the rotating propeller a time step was chosen so that the propeller was rotating less than 1° per time step.

The simulations dealing with cavitational flow employed a Volume of fluid (VOF) multiphase model using the SST k-Omega turbulence model which solves the Wilcox k-omega model in the near wall flow. For solving the far field flow the k-epsilon model is solved which takes advantage of its free stream independence. The turbulence model change is done by introducing a switching function as a factor to the original governing equations. The blending between both models takes place in boundary layer wake region. The governing equations can be found in (Menter, 1994).

To predict cavitation the VOF model allows the flow to consist of two phases whereas its spatial distribution in time is defined by a volume fraction variable. The model assumes that the fluid is homogenous so that both phases share the same properties, such as velocity and pressure. In order to accurately model the interaction between the phases the numerical mesh resolution should be sufficiently fine, at least three cells covering one vapour bubble, as shown in Figure 2. (CD-adapco, 2015)

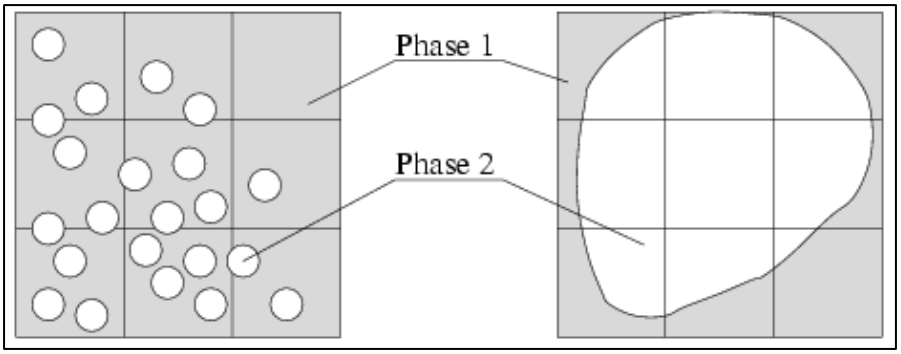

Figure 2 - Grid requirements for the VOF model (CD-adapco, 2015)

Predicting cavitation requires modelling a change of state. The mathematical description is given by the “Sauer and Schnerr Cavitation Model” published in 2001 (Schnerr and Sauer, 2001). It is based on the “Full cavitation model” proposed by Singhal (Singhal et al., 2001) which is using the Rayleigh equation (4), controlling the bubble radius DR of the vapour bubbles, which are depending on the saturation pressure p_S, the local pressure p and the liquid density ρ_L.

$$\frac{DR}{Dt} = sign(p_S - p)\sqrt{\frac{2}{3}\frac{|p_S - p|}{\rho_L}} \tag{4}$$

The equation of the volume fraction of vapour (5) describes the two phase model, namely the water phase and the vapour phase. Both phases are part of a single fluid. In order to mix both phases with respect to their length scales the Eulerian Multiphase Model is used.

$$\frac{d}{dt}\int_V \alpha_V \, dV + \int_S \alpha_V \, (\vec{v} - \vec{v}_S) \cdot \vec{n} \, dS = \int_V q_V \, dV \tag{5}$$

To define the generation of vapour in the water, this cavitation model introduces the volume fraction of vapour in a certain control volume (6). To initialise the generation of vapour the model has two main parameters, namely the number of bubbles in a certain volume fraction of the liquid n_0 and the initial bubble radius R. (Peric et al., 2013)

$$\alpha_V = \frac{V_V}{V_V + V_L} = \frac{\frac{4}{3}\,\pi\,R^3\,n_0}{1 + \frac{4}{3}\,\pi\,R^3\,n_0} \tag{6}$$

Furthermore the growth rate of the bubble volume over time has to be controlled. This is done by equation (7).

$$\frac{DV_B}{Dt} = 4\,\pi\,R^2\,\frac{DR}{Dt} \tag{7}$$

To make sure that there is an information exchange between both phases, it is necessary to define a primary phase (continuous) and a secondary phase (bubbles) which is dispersed in the primary phase. The interaction of both phases is handled by passing a momentum from one phase to the other. Using this approach it is possible to calculate drag and lift forces. (CD-adapco, 2015)

3. TWISTED DELFT HYDROFOIL

The Twisted Delft Hydrofoil was chosen as it was considered to be an easier simulation task compared to the PPTC in terms of mesh size and simulation time. The cavitation test for the hydrofoil was performed in the cavitation tunnel at Delft University of Technology by Foeth in 2008 (Foeth, 2008). The experimental results are publicly available what makes it a standard test case to validate and calibrate numerical simulation of cavitation. Figure 3 shows the experimental setup of the foil in the cavitation tunnel test section. It has a span of $0.3\ m$ being symmetrical to its midsection. The angle of attack varies between $-2°$ and $9°$ at the midsection. This causes the development of cavitational flow on the suction side of the foil.

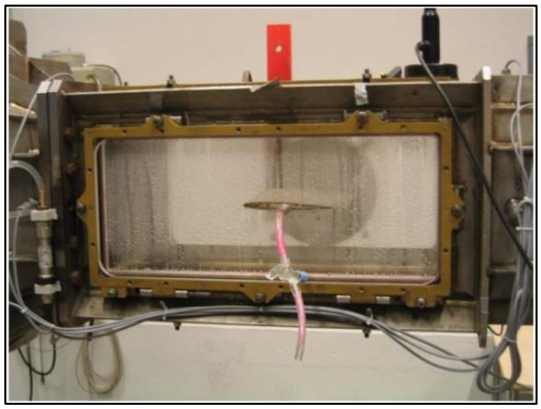

Figure 3 - Experimental setup of the Delft Hydrofoil (Hoekstra, 2007)

The test results (available at: http://maritimetechnology.tudelft.nl/SHS/) include local pressure measurements on the hydrofoil surface and lift force measurements. The results to consider for the present simulation can be found in (Delft-University-of-Technology, 2010).

3.1 NUMERICAL DOMAIN

As the resulting flow is assumed to be ideally symmetrical with respect to the midsection the numerical domain therefore covers only half of the wing. This results in less time-expensive computations. The domain boundaries were defined as velocity inlet and a pressure outlet, a symmetry plane at the midsection of the foil and walls for the top, the bottom, the side and the foil itself. Figure 4 gives an impression of the numerical domain, showing the foil in red and the outlines of three refinement regions inside the domain in green.

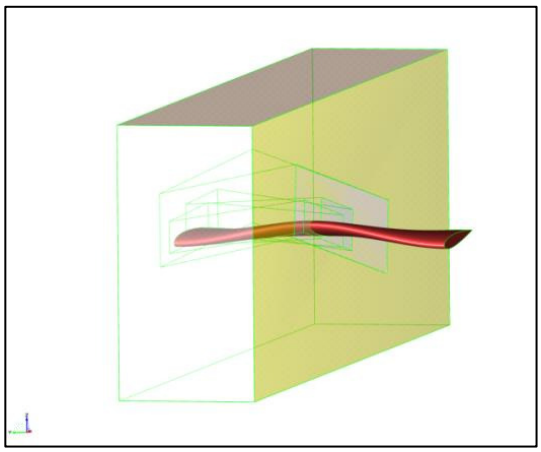

Figure 4 - Numerical domain for the Delft Hydrofoil

The generated volume mesh is composed of cuboid cells. Defining refinement regions allowed creating a denser mesh where it is necessary in order to solve the flow more accurately. To keep the mesh size as small as possible, the refinement regions follow the foil's angle of attack, thus still surrounding the foil surface and the suction side widely in order to cover the cavitating flow area. The shapes were created in FRIENDSHIP Systems software CAESES, which provides an advanced 3D geometry modeller. Figure 5 shows a plane cut of the common approach using simple volume blocks for the refinement region (top) and the present shape depending approach (bottom).

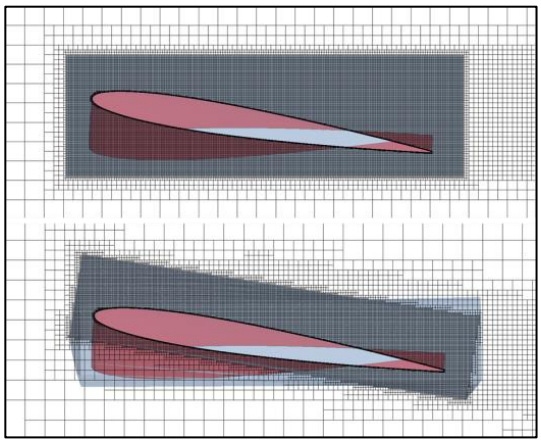

Figure 5 - Simple block refinement mesh (top) and shape depending refinement mesh (bottom)

The comparison shows a quite high difference in the total number of cells (Table 1). The reduction of 32.3 % of mesh size helps to avoid solving unnecessary dense meshes which results in shorter simulation times.

Table 1 - Comparison of number of cells of different refinement meshing approaches

	Simple Block Refinement	**Shape Depending Refinement**	**Difference** [%]
No. of Cells	10.509.766	7.111.319	32.3

3.2 FULLY WETTED FLOW – RANSE SIMULATIONS

Fully wetted flow RANSE simulations, based on the settings shown in Table 2 were run to find a suitable numerical setup to match the test experimental results of test case 2. After running different mesh sizes the presented numerical mesh and physical settings were found to give accurate results.

Table 2- RANSE simulation settings

Geometry	**TWIST 11 HYDROFOIL** (Case 2)
Angle of Attack	-2°
Condition	Fully Wetted
Chord Length	$0.15\ m$
Span	$0.15\ m$
Tunnel Domain	0.6 x 0.15 x $0.3\ m$
Mesh	Cuboid Cells
Number of Cells	7.111.319
Number of Prism Layers	10
Initial Conditions	
Inlet Velocity	$[6.97, 0, 0]\ \frac{m}{s}$
Outlet Pressure	$97\ kPa$

The lift force and the pressure coefficient at different stations on the foil surface were validated according to the values measured in the test case 2. After convergence the lift force on the foil was

found to be close to the experimental result (see Table 3). The experimental lift force was calculated by using a recommended quadratic function $Lift = 10.052 \cdot flow\ speed^2$.

Table 3 - Lift force of EFD and CFD for RANSE simulation

	EFD	**CFD**	**Deviation** [%]
Lift Force [N]	488.34	491.5	0.65

Figure 6 shows where the pressure probes were located on the foil surface in the experiments. For the probe points 2-9 (50% span), 10-15 (60% span) and 16-18 (70% span) the simulation results are in good agreement with experimental measurements.

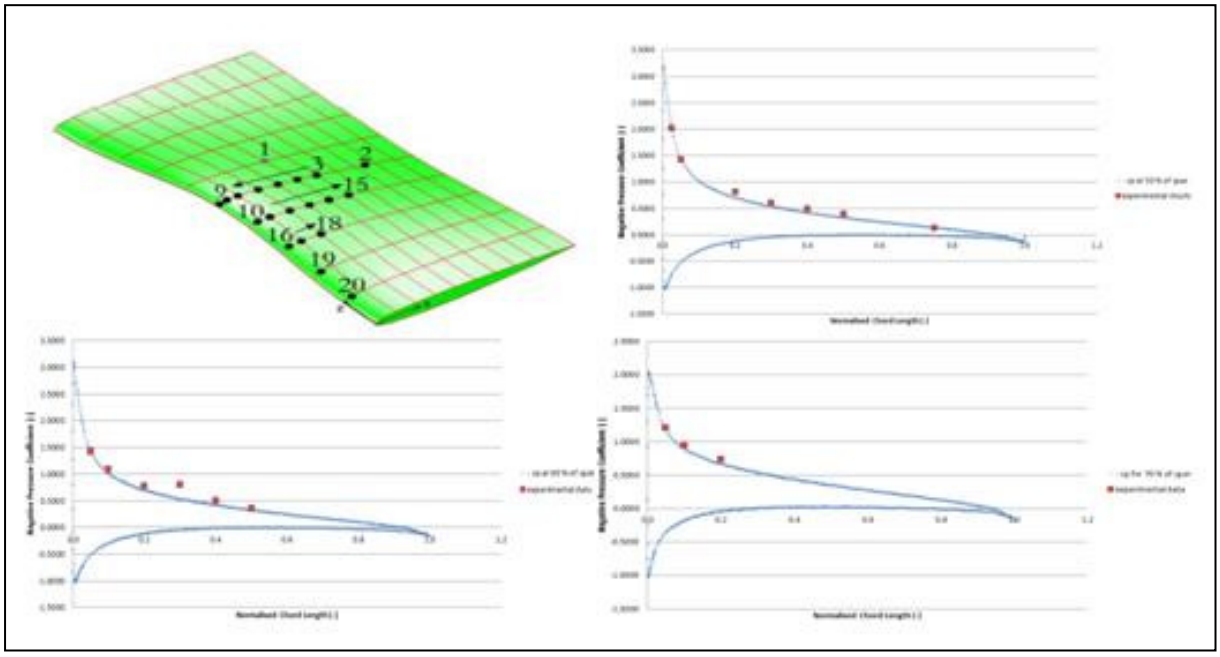

Figure 6 – Pressure probes on foil (source) and pressure coefficient distribution on the foil surface at 50%, 60% and 70% of the span (EFD: red, CFD: blue)

3.3 CAVITATIONAL FLOW – RANSE & DETACHED-EDDY SIMULATIONS

The same numerical mesh size was used to run the cavitational flow RANSE simulations. In order to be able to simulate cavitation the VOF solver was added. To check whether the numerical mesh is sufficient enough or not to resolve the small scale eddies in the detached-eddy simulations, additional functions were added to the RANSE simulation as described in section 2. Figure 7 shows the visualisation of the turbulence length ratio for $r_l \geq 1$. On the LHS the function is applied as recommended with the factor $a = 2$. The visualisation indicates that the mesh is not fine enough to resolve the small scale flow. Reducing the factor a to the value of $a = 0.025$ seems to give accurate results for the detached-eddy simulations. This reduction would increase the number of cells by a factor of 80 in each spatial direction. Even if one would apply the mesh refinement only to the most inner refinement region, the total number of cells would be unreasonable high (considering the already high number of 7.111.319 cells).

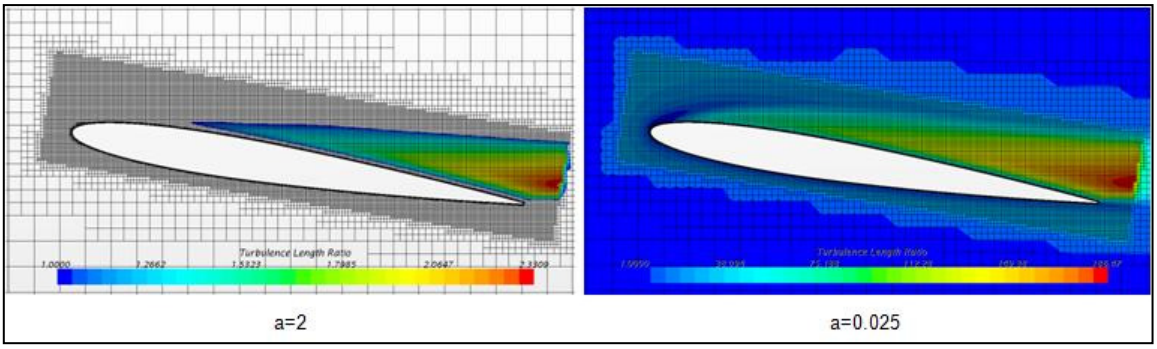

Figure 7 - Turbulence length ratio $r_l \geq 1$ on mesh plane for cavitational flow RANSE simulation (LHS: $a = 2$, RHS: $a = 0.025$)

Considering the visualisation of the turbulence length ratio in Figure 1 (RHS) the grid at the leading edge of the foil, where the value of r_l is close to one, was further refined for the detached-eddy simulations as this region on the foil surface is the inception point for the cavitation development. Figure 8 shows a comparison of cavitation by visualising the vapour phase on the foil surface. The RANSE simulation predicted cavitation starting at the leading edge of the foil covering around 60% of the foil in span-wise direction. This is in good agreement with the experiments. As expected the RANSE simulation did not show any detached cavitation, whereas the detached-eddy simulation predicted cavitation detached from the foil surface travelling downstream.

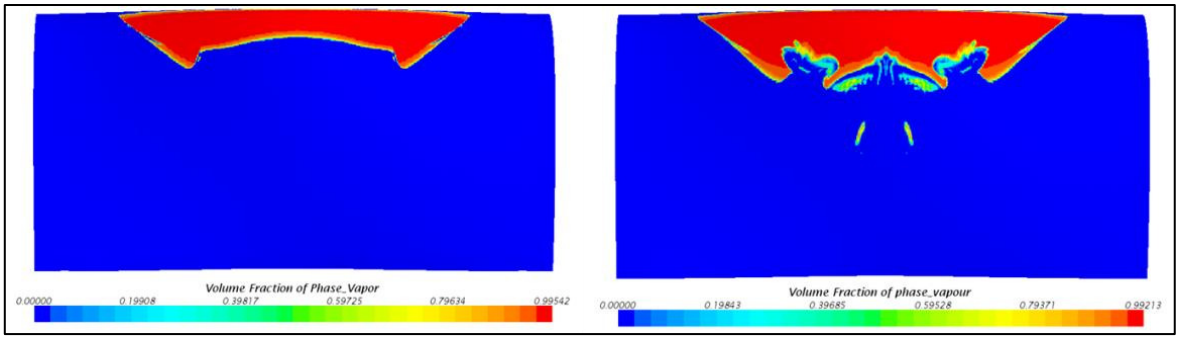

Figure 8- Cavitation on foil (LHS: RANSE simulation, RHS: Detached-eddy simulation)

Analysing the cavitation properties revealed that the average of the cavitation rate in the RANSE simulation is higher compared to the stable cavitation on the foil surface in the detached-eddy simulation. Table 4 shows the average cavitation rate as well as the peak range of both simulations. As the RANSE simulation did not predict detached cavitation the overall rate is nearly constant resulting in a small peak range as well. The detached-eddy simulation however predicted a higher peak range, also shown in Figure 9 (top diagrams). This is clearly related to the pronounced change of the cavitation volume.

Table 4 - Cavitation rate of RANSE and detached-eddy simulations

	Average of cavitation rate $\left[\frac{1}{s}\right]$	**Peak range of cavitation rate** $\left[\frac{1}{s}\right]$
RANSE simulation	16060	160
Detached-eddy simulation	15100	9000

Figure 9 compares the cavitation rate with the lift force and the drag force respectively, derived from the detached-eddy simulation. Due to the less pronounced peak range of the cavitation rate in the RANSE simulation, no strong relations between the cavitation and the forces were found. By contrast,

the detached-eddy simulation predicted a stronger relation between cavitation, lift and drag. With most of the peaks of cavitation the drag increased as well, whereas the lift of the foil decreased.

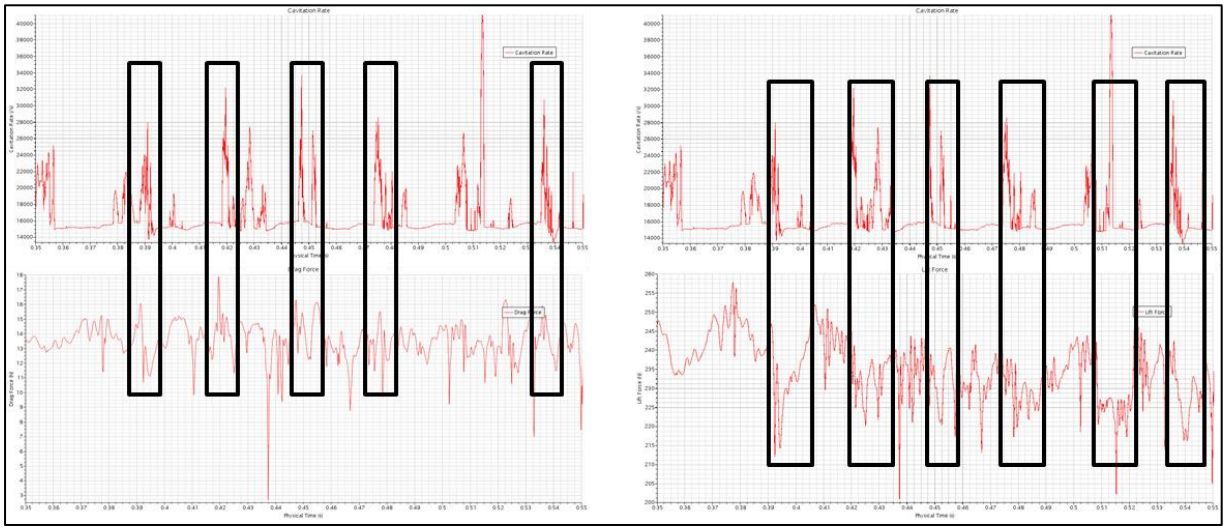

Figure 9 - Dependency between cavitation rate (top LHS and RHS) and lift (bottom RHS) and drag forces (bottom LHS) over time, derived from the detached eddy simulation

Figure 10 gives an impression of the cavitational volume in time predicted in the detached-eddy simulation by visualising an iso-surface of the volume fraction of vapour with an iso-value of 0.5. This type of simulation was able to capture the cavitation travelling downstream along the foil surface as well as detached cavitation above the foil. Comparing the snapshots with movie recorded in the experiments showed that the cavitation predicted in the simulation is in good agreement with the experiments.

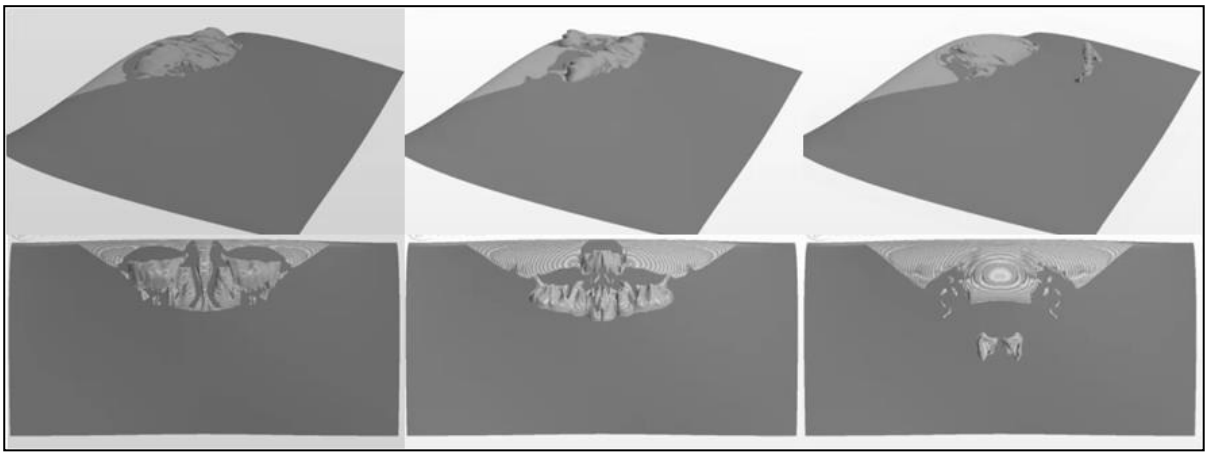

Figure 10 - Cavitation volume on the foil by visualising an iso-surface of the volume fraction of vapour in perspective view (top) and top view (bottom), derived from the detached-eddy simulation

4. POTSDAM PROPELLER TEST CASE (PPTC)

After the Delft Hydrofoil simulations, a more complex test case was chosen to compare RANSE and detached-eddy simulations. The Potsdam Propeller Test Case (PPTC) is such a test case. The Potsdam Model Basin SVA provided experimental test data for open water tests and cavitation tests. The VP1304 model propeller, a five bladed controllable pitch propeller with a diameter of $D = 0.25\,m$,

was designed to generate a tip vortex as can be seen in Figure 11. The results are available at http://www.sva-potsdam.de/pptc_data.html.

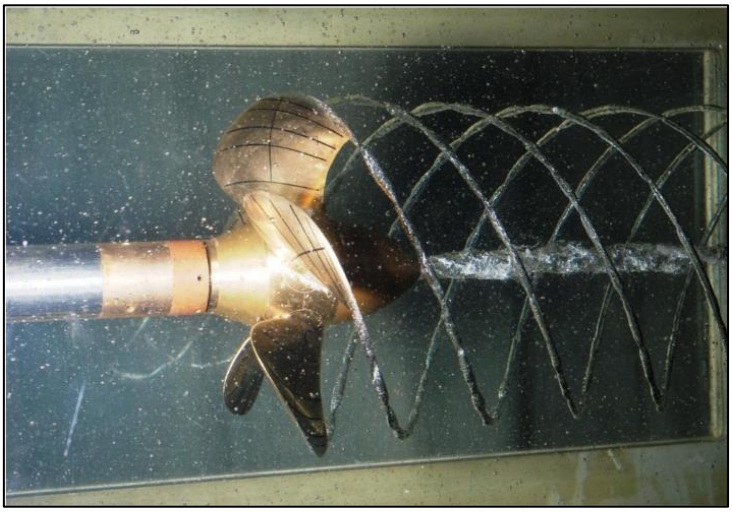

Figure 11 - Potsdam Propeller Test Case in the cavitation tunnel

The numerical simulations refer to the test case 2.3.1. The conditions and the resulting thrust coefficient are shown in Table 5. For this test case only cavitational flow simulations were performed.

Table 5 - Test conditions and measured thrust coefficient

Advanced Coefficient	1.019
Number of revolutions	24.987 $\frac{1}{s}$
Resulting inflow speed	6.365 $\frac{m}{s}$
Cavitation number	2.024
Thrust coefficient	0.387

4.1 NUMERICAL DOMAIN

The numerical domain consists of a static domain representing the cavitation tunnel and a rotational domain around the propeller employing a sliding mesh approach. The domain boundaries were defined as velocity inlet and pressure outlet. The tunnel wall as well as the propeller was defined as wall type. The rotating domain passes through the gap between shaft and hub.

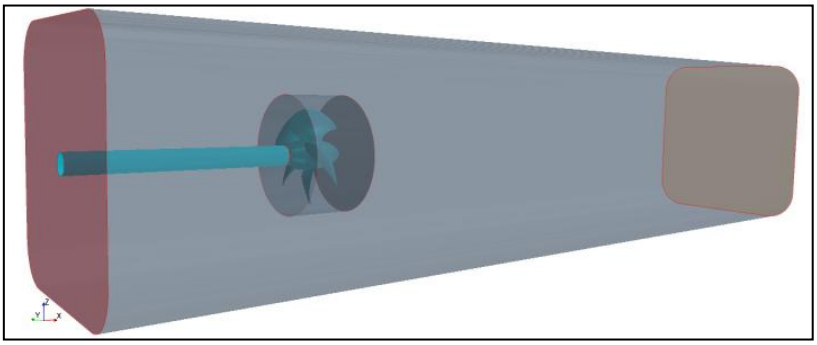

Figure 12 - Numerical domain of the PPTC

In order to avoid an unnecessary high number of cells, several refinement regions were set around the propeller, inside the rotational domain, at the hub tip and the blade tips. This was done to refine

the regions were cavitation was expected (see Figure 13). After a few different mesh settings were tested, the resulting mesh for the RANSE simulation consisted of 7.552.004 cells.

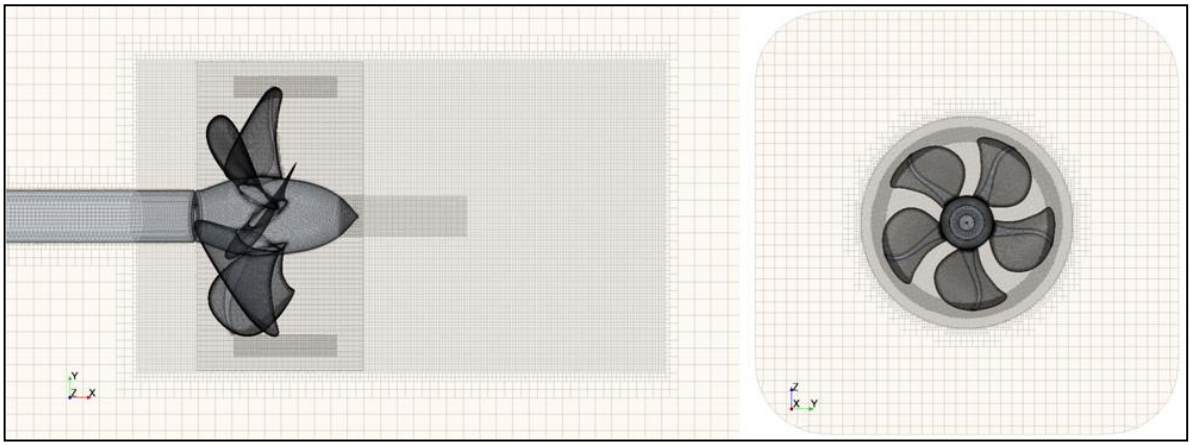

Figure 13 - Mesh refinements at blade tips and hub (LHS: side view, RHS: front view)

4.2 CAVITATIONAL FLOW – RANSE AND DETACHED-EDDY SIMULATIONS

The results to consider were the thrust coefficient and the location and extension of cavitation on the propeller and in the wake. After convergence the thrust coefficient was found to be within an acceptable range compared to the experimental results (see Table 6).

Table 6 - Thrust coefficient of EFD and CFD for RANSE simulation

	EFD	**CFD**	**Deviation** $[\%]$
Thrust Coefficient $[-]$	0.387	0.3702	-4.3

In order to prepare the detached-eddy simulation, the same procedure as in section 3.2 was used. Therefore the turbulence length ratio was analysed to find out if the small scale flow was solved accurately. When visualising the turbulence length ratio for the factor value of $a = 2$, only a small spot directly downstream of the propeller hub tip showed a value of $r_l \geq 1$. Reducing the value to $a = 0.07$ would provide a sufficient fine mesh in order to solve even the smallest scales of the flow.

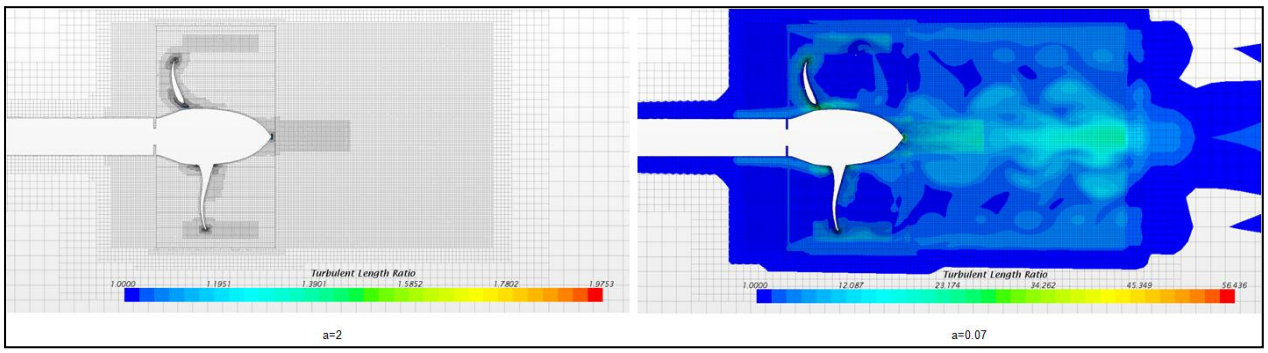

Figure 14 - Turbulence length ratio $r_l \geq 1$ on mesh plane for cavitational flow RANSE simulation (LHS: $a = 2$, RHS: $a = 0.07$)

This reduction would increase the number of cells by a factor of 29 in each spatial direction. Again, similar to the previous test case, it would have been impractical to refine the mesh by that factor. Nevertheless, the numerical mesh for the detached-eddy simulation was further refined. The resulting

mesh consisted of $13.941.753$ cells. Although the detached-eddy simulations showed no considerable improvement in the thrust coefficient the visualisation of velocity, pressure and cavitation showed an improvement compared to the RANSE simulations.

Table 7 - Thrust coefficient of EFD and CFD for Detached-eddy simulation

	EFD	**CFD**	**Deviation** $[\%]$
Thrust Coefficient $[-]$	0.387	0.3705	-4.3

Especially the hub vortex is pronounced in the detached-eddy simulations as can be seen in the following figures. The velocity field as well as the pressure field are visualised on a plane in the flow domain. Both visualisations showed reasonable results. It should be highlighted that Figure 15 as well as Figure 16 show the generation and the downstream-developed of the propeller blade tip vortex fairly well.

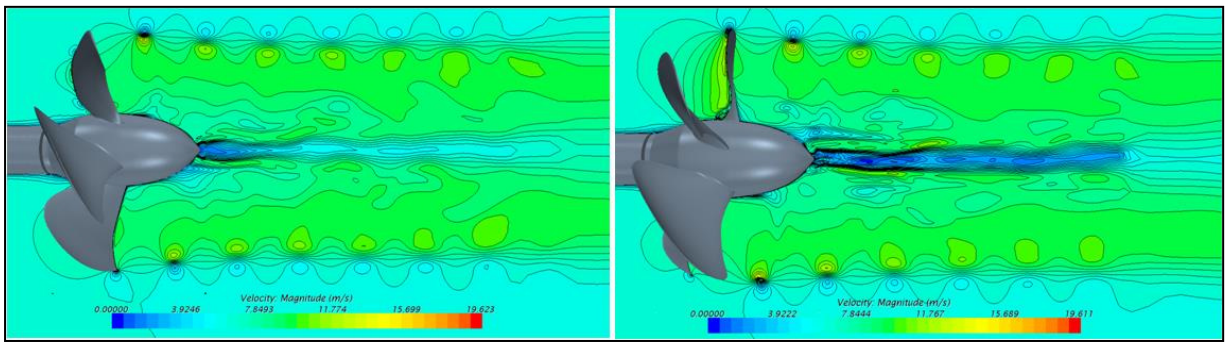

Figure 15 - Velocity Field (LHS: RANSE simulation, RHS: Detached-eddy simulations)

Due to the sliding mesh approach the interfaces between the static domain and the rotational domain introduced a numerical error in the pressure field. This is shown in Figure 16 as the interface boundaries are clearly visible. This was probably caused by the slightly change of cell size between the rotational and the static domain.

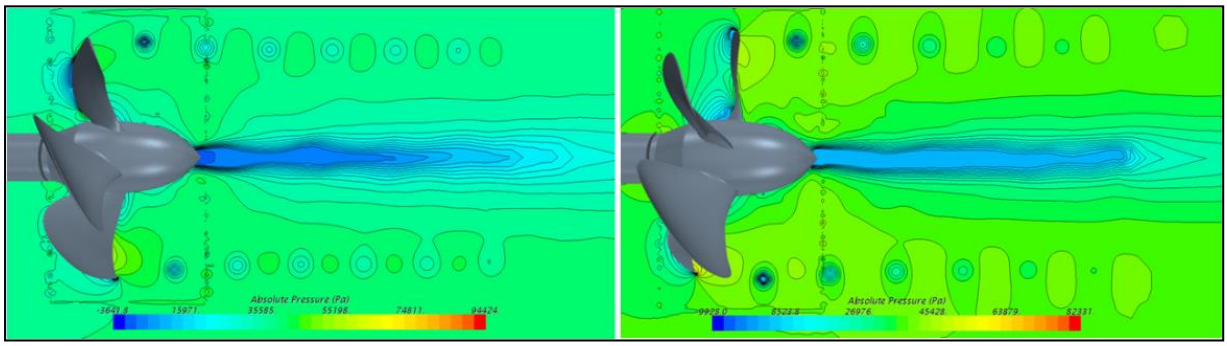

Figure 16 - Pressure Field (LHS: RANSE simulation, RHS: Detached-eddy simulations)

Figure 17 shows the visualisation of an iso-surface of the volume fraction of vapour for an iso-value of 0.5. The prediction of the location of cavitation on the propeller geometry is close to the experimental results for both simulations (compare Figure 11 and Figure 17). The sheet cavitation on the propeller blades occurred at the blade leading edges up to the blade tips and the blade roots. In both simulations the amount of cavitation on the blades is over predicted. The hub vortex predicted in the RANSE simulations showed a clear dependency on the mesh cell size, whereas this dependency was much weaker in the detached-eddy simulations. The RANSE simulation showed no detached

cavitation for the iso-value of 0.5. The detached-eddy simulations predicted the shedding cavitation leaving downstream from the blade tips within the blade tip mesh refinement.

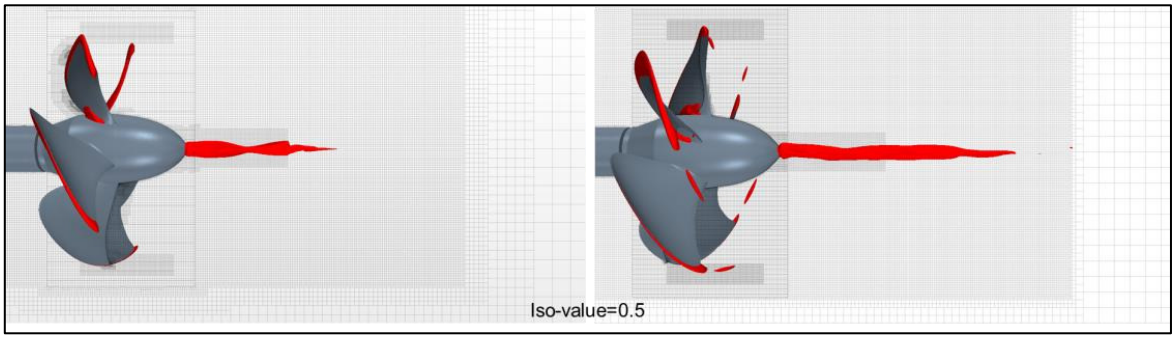

Figure 17 - Cavitation on the propeller and in the wake flow by visualising an iso-surface of the volume fraction of vapour (LHS: RANSE simulation, RHS: Detached-eddy simulations)

5. CONCLUSIONS

The application of a numerical mesh test, in order to define a mesh which would be able to solve the smallest turbulent scales of the flow, indicated that the necessary density of the mesh for detached-eddy simulations would be impracticable high. Although the recommendations of the mesh test were violated, the detached-eddy simulations showed reasonable results when compared to the experimental findings. Furthermore a more advanced shape depending meshing procedure for refinement regions was tested successfully, resulting in a mesh size reduction of 30%. In order to avoid numerical errors on the sliding mesh interface in the propeller simulations an additional prism layer could be added which would align the cells normal to each other.

The simulation of the Delft Hydrofoil showed a strong dependency between the cavitation rate and the lift and drag forces when using the detached-eddy model. The RANSE simulations however were not able to capture these dependencies as the sheet cavitation on the foil surface was highly stable. This caused the cavitation rate to be higher in average in the RANSE simulations. It follows that rely on RANSE simulations for predicting cavitating flow would lead to misleading conclusions in terms of cavitation volume and frequency.

It has been shown that the accurate numerical simulation of cavitational flow on a hydrofoil as well as on a marine propeller requires the use of an advanced turbulence model such as the SST k-omega detached-eddy model. Although the RANSE simulations were able to predict thrust and drag forces in the same acceptable range, the development of turbulent cavitational flow was under predicted. Especially the shedding cavitation, causing vibration and erosion of downstream located structures (e.g. ship hull and rudder), was not captured in the RANSE simulations. This makes detached-eddy simulations a powerful alternative and an indispensable tool for predicting the impact of cavitational flow on various parameters such as propeller efficiency and propeller noise.

Acknowledgement

Results were obtained using the EPSRC funded ARCHIE-WeSt High Performance Computer (www.archie-west.ac.uk). EPSRC grant no. EP/K000586/1.

REFERENCES

ASHTON, N., REVELL, A., SKILLEN, A., POLETTO, R., BILLARD, F. & LAURENCE, D. 2014. Progress in Tools for Turbulence Modeling and Simulation. The University of Manchester & CD-adapco.

BOORSMA, A. & WHITWORTH, S. 2011. Understanding the Details of Cavitation. *2nd International Symposium on Marine Propulsors smp'11.* Hamburg.

CD-ADAPCO 2015. STAR-CCM+ User Guide Version 9.06.011.

DELFT-UNIVERSITY-OF-TECHNOLOGY 2010. Pressure and Lift Measurements on the Twist 11 Hydrofoil. Delft University of Technology.

FOETH, E. J. 2008. *The structure of three-dimensional sheet cavitation.* PhD, Technische Universiteit Delft.

HOEKSTRA, M. 2007. Delft Twist 11 foil. *VIRTUE WP4 Workshop.* Wageningen, Netherlands.

ITTC. 2011. ITTC- Recommended Procedures and Guidelines - Practical Guidelines for Ship CFD Applications.

MENTER, F. R. 1994. Two-Equation Eddy-Viscosity Turbulence Models for Engineering Applications. *AIAA Journal,* 32.

MUSCARI, R., MASCIO, A. D. & VERZICCO, R. 2012. Modeling of vortex dynamics in the wake of a marine propeller. *Elsevier Ltd,* Computers & Fluids 73**,** 15.

PERIC, M., SCHAEFER, F., SCHRECK, E. & SINGH, J. 2013. Application of STAR-CCM+ in Marine and Offshore Engineering: State-of-the-Art and New Developments. .

SALVATORE, F., STRECKWALL, H. & TERWISGA, T. V. Propeller Cavitation Modelling by CFD – Results from the VIRTUE 2008 Rome Workshop. First International Symposium on Marine Propulsors smp'09, 01.06.2009 2009 Trondheim, Norway. 10.

SCHNERR, G. H. & SAUER, J. 2001. Physical and Numerical Modeling of Unsteady Cavitation Dynamics. *4th International Conference on Multiphase Flow, New Orleans, USA*.

SINGHAL, LI & ATHAVALE 2001. Mathematical Basis and Validation of the Full Cavitation Model. *ASME FEDSM'01 New Orleans, Louisiana, 2001.*